



Kinetics of fluoride adsorption onto native and Mg(OH)₂-amended limestone

Noura AL-Darwish¹ · T. M. Abu-Sharar¹

Received: 5 December 2020 / Accepted: 1 January 2021 / Published online: 30 January 2021
© The Author(s) 2021

Abstract

The adsorption kinetics of fluoride onto limestone (LS) and Mg(OH)₂-amended LS were investigated using batch adsorption technique. Data were best fitted to second-order and Elovich models. The Mg(OH)₂-amended LS showed substantial increases in F⁻ adsorption relative to native LS. Similarity of ionic radii and charge of both F⁻ and OH⁻ were hypothesized to be the major cause of such increases. The OH⁻ functional group of the surface Mg(OH)₂ could be exchanged by aqueous F⁻ through surface complexation (ligand exchange). No background effect of naturally occurring anions in F⁻-rich groundwater on adsorption capacity of Mg(OH)₂-amended LS. The results reveal that the Mg(OH)₂-amended LS can be environmentally safe and economical for F⁻ removal.

Keywords Drinking water · Ligand exchange · Pollution · Limestone · Wadi al-yutum water · Jordan

Introduction

Shortage in fresh water supply in Jordan has been in steady increase due to high-population growth rate, socioeconomic development, poor management of water resources and the resultant contamination of these resources by a myriad of pollutants (Abu-Sharar 2005). One of these pollutants is fluoride which can be detected in appreciable levels in different water resources as a product of weathering of the bearing minerals. Ground waters with high F⁻ concentrations are reported in many areas of the world (Ahn 2012; Karro and Uppin 2013). In such areas, water enrichment with F⁻ is thought to be the root cause of many diseases. According to the World Health Organization (WHO 2008), the maximum acceptable concentration of F⁻ in drinking water must be less than 1.5 mg L⁻¹ but the safe limit should be less than 1.0 mg L⁻¹. Fluoride consumption in small amounts is usually beneficial for normal mineralization of bones and formation of dental enamel, while long term consumption of water containing excessive amounts of F⁻ can

lead to dental fluorosis, mottling of teeth, and softening of bones (Gbadebo 2012; Davraz et al. 2008). For these reasons, removal or lowering of excessive F⁻ concentration in drinking water is important in terms of public health and environmental safety.

High levels of F⁻ in groundwater were reported in different locations in Jordan. These include Wadi Al-Yutum of southern port city of Aqaba. The F⁻ concentration in these well waters exceeds the threshold limit of 1.5 mg L⁻¹. Major water supply to Aqaba city comes from the fossil water of Disi aquifer (Farhan and Anaba 2016). This resource is endangered by depletion as a result of increasing urbanization in the city itself and transportation of huge volumes (~100 × 10⁶ m³ yr⁻¹) to the capital city of Amman. Subsequently, the need for additional water resources has been escalating. The high cost of other water resources like sea water desalination imposes the need to focus on low cost methods of F⁻ removal from essentially potable water.

Numerous de-fluoridation methods of F⁻ from drinking water to acceptable limits have been reported. Most of these methods were based on adsorption techniques (Tikki 2014). Other methods utilized reverse osmosis (Wang et al. 2015), electro dialysis (Gmar et al. 2015), nanofiltration (Mnif et al. 2010), but all of them were almost abandoned due to the high cost of investment and maintenance. Precipitation techniques are usually applied for F⁻ removal from very highly contaminated industrial wastewater but are

✉ Noura AL-Darwish
phdnoura@gmail.com

T. M. Abu-Sharar
t.m.abu-sharar@ju.edu.jo

¹ The University of Jordan-Amman, Amman, Jordan

hardly applied to groundwater because of its low efficiency in reducing F^- concentration to $1\text{--}2\text{ mg L}^{-1}$ (Ezzeddine et al. 2015; Chang and Liu 2007). Other methods like Nalgonda precipitation was discarded since it could add harmful contaminants to water and may require pH adjustment (Waghmare and Arfin 2015). Metallic iron packed beds (Fe filters) were tested for defluorination (Nde-Tchoupe et al. 2019; Heimann et al. 2018). The results demonstrated a relatively low adsorption capacity of iron corrosion products, while those based on co-precipitation/flocculation were better suitable. Since F^- -adsorption is selective, easily handled, low-cost and effective, several adsorbents were examined (Tikki 2014; Habuda-Stanic et al. 2014). Those included activated alumina (Khichar and Kumbhat 2015), calcite (Budyanto et al. 2015; Turner et al. 2005; Ali 2013; Dutta, and Nath 2010; Padhi and Tokunaga 2015), magnesia (Xu et al. 2012; Aravind and Elango 2006), and clay (Vinati et al. 2015). Additionally, Medellin-Castillo et al. (2015) and Jayarathne et al. (2015) examined bone char (hydroxyapatite) for F^- adsorption from water. Rare earth metal adsorbents have been widely studied as potential F^- adsorbent because of their high adsorption capacity. However, high price and low adsorption performance in neutral or alkaline condition largely limited their usage (Ma et al. 2014).

Many researchers brought about several modifications of common adsorbents to improve their adsorption capacities, and thus, to lower F^- equilibrium concentration below the former threshold limit in drinking water. For example, modification of commercial granular activated carbon with lanthanum oxyhydroxides increased F^- adsorption capacity by five times as compared to unmodified carbon (Vences-Alvarez et al. 2015). Similarly, Al-modified hydroxyapatite possessed high F^- -adsorption capacity due to more abundant surface hydroxyl groups (Nie et al. 2012). Jain and Jayaram (2009) modified LS with Al-hydroxide to get some improvement on F^- adsorption capacity. Ma et al. (2014) used Biocarbon-Mg/Al layered double hydroxides composites to improve F^- adsorption. Using Al in modification processes might increase threats of elevated Al concentrations in the reclaimed water. Therefore, there has been an increasing need to modify adsorbents using non toxic materials. Different nontoxic MgO materials have been evaluated for improvement of F^- adsorption onto commercial MgO; synthesized pillar and microsphere-like MgO (Lee et al. 2017), nano-sized MgO (Devi et al. 2012), synthesized meso MgO (Yu et al. 2018), porous MgO nanoplates (Jin et al. 2016). Adsorption capacity of the porous MgO nanoplates was superior to other MgO nanomaterials. Adsorption was rapid in the first 20 min and resulted in adsorption capacity of more than 97% of the initial F^- -concentration. Similarly, meso MgO exhibited excellent performance in removing F^- . The high surface area and multi-size pore structure made synthesized MgO a potentially excellent adsorbent of F^- .

The main limiting step for de-fluoridation using MgO was the step of MgO hydrolysis to form $Mg(OH)_2$ (Margandan et al. 2014).

This study was designed to evaluate the kinetics and magnitude of F^- removal from aqueous phase using locally available native and $Mg(OH)_2$ -amended LS. This Ca and Mg-based adsorbent is nontoxic, economic, environment-save, and direct without the extra step of MgO hydrolysis.

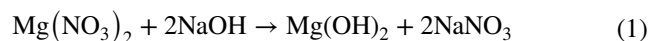
Materials and methods

Material

Local LS samples were collected from two mines in Central Jordan. Fluoride standard solution (1000 mg L^{-1}) was used to prepare solution samples using distilled water. Other chemicals used in the experiments; $Mg(NO_3)_2$ and NaOH were all of analytical grade and obtained from Sigma-Aldrich (USA), or Merck KGaA (Germany).

Experimental methods

Limestone samples were screened, washed with de-ionized water to remove dirt and impurities, and then dried at about $105\text{ }^\circ\text{C}$ for 24 h. The dried LS samples were ground and sieved to pass $50\text{ }\mu\text{m}$ mesh. Subsamples from the native LS samples were impregnated with $Mg(OH)_2$ using amended method of Jain and Jayaram (2009). Here, a subsample of 15.0 g from each native LS sample was added to 1 L solution which was made by mixing 500 ml of 0.01 M NaOH with another 500 ml of 0.10 M $Mg(NO_3)_2 \cdot 6H_2O$ (Magnesia-1 and Gama-1). In case of Magnesia LS sample, additional double strength OH-amendment was performed using 500 ml of each 0.02 M NaOH and 0.20 M $Mg(NO_3)_2 \cdot 6H_2O$ solutions (Magnesia-2). The resultant suspension was stirred for six hours then left standing still for 24 h at room temperature. The reaction of these two chemicals produced highly soluble $NaNO_3$ and relatively insoluble $Mg(OH)_2$:



The precipitate of magnesium impregnated LS was separated from the slurry by vacuum filtration; then, the solid was washed with distilled water, dried for 24 h at $105\text{ }^\circ\text{C}$, and stored in reagent bottle for later use. The dried slurry was in friable form that did not require any additional grinding.

To separate any possible F^- adsorption onto $Mg(OH)_2$ particles, the same standard NaOH and $Mg(NO_3)_2$ solutions were mixed and left standing still overnight then any possible solid phase formations of $Mg(OH)_2$ colloidal particles were separated using the same micro-pore filter. The

filter paper was dried in a manner analogous to previous treatment of amended LS, and no appreciable change in the weight of the filter paper following the filtration process was recorded.

Kinetics of F^- adsorption using native and amended LS were experimented using the batch method described by Alagumuthu et al. (2010). Thirty ml of F^- standard solution (10 mg L^{-1}) were pipetted to each of nine duplicate centrifuge tubes then 3 g of the specified LS sample were added to each solution. The suspensions were shaken using Vortex shaker at 1000 rpm for a specified time period (10, 15, 30, 60, 240, 600, 1440, 2880, and 4320 min) at room temperature ($25 \pm 1 \text{ }^\circ\text{C}$) and pH of 6.2 for all experiments. Solutions were then separated from the solid phase using centrifugation at 3600 rpm for 5 min. The resultant supernatant solutions were further filtered using $0.45 \text{ }\mu\text{m}$ syringe nylon-membrane filter, and F^- was analyzed using ion chromatography.

Analytical methods

Several chemical and physical analyses were performed on LS and water samples. Fluoride concentration was determined using Metrohm 871 Bioscan ion chromatograph, while analysis for calcium, magnesium and heavy metals were carried out using Savant AA GBC atomic absorption spectrometer. Limestone surface area was determined using NOVA 2200e surface area and pore size analyzer, and particle size distribution was measured using Malvern MasterSizer 2000. Additionally, LS subsamples were subjected to spectral analyses including fluorescence analysis of X-rays using Shimadzu EDX-7000, Fourier transform infrared spectra (FTIR) using Thermo Nicolet 670, and scanning electron microscopy (SEM) using FEI Inspect F50 high-resolution electron microscope.

Results and discussion

Characterization of natural and amended limestone

Results of chemical analyses performed on the amended and native LS subsamples showed similar purity for all LS samples, while some differences appeared in the impurities; sulfate, silica, organic content, chloride, iron and aluminum as shown in Table 1. The presence of charged iron and aluminum, and low content of F^- is expected to increase F^- adsorption on all LS subsamples. The metal oxides reported in the literature for defluoridation include Fe, Mn, Al, Ca, and Mg oxides (Nde-Tchoupe et al. 2019; Nie et al. 2012; Markovic et al. 2009).

Amendment of LS subsamples caused no changes in their chemical composition except for Mg which was added to the

Table 1 Results of chemical analysis of native and amended LS subsamples

Analysis	Native LS		Amended LS		
	Magnesia	Gama	Magnesia-1	Magnesia-2	Gama-1
	wt/wt %				
H ₂ O	0.97%	0.27%	0.50%	0.65%	0.42%
Ca	39.40%	39.50%	39.30%	39.40%	39.50%
SO ₄	0.08%	0.47%	0.08%	0.08%	0.42%
Purity	98.38%	98.66%	98.30%	98.40%	98.62%
SiO ₂	0.18%	0.47%	0.18%	0.17%	0.42%
P	0.04%	0.04%	0.04%	0.04%	0.04%
Na	0.02%	0.01%	0.01%	0.01%	0.01%
	mg kg ⁻¹				
Fe	130	40	129	127	37
Al	360	110	350	345	105
Mg	110	170	400	830	440
Cl	610	61	58	63	57
N	187	142	206	220	163
COD	220	65	220	218	61
F	71	58	69	65	53

surface of the subsamples in the form of $\text{Mg}(\text{OH})_2$ through the amendment procedure. Some decreases in Cl and Na concentrations of Magnesia LS were observed as a result of the washing steps.

X-ray fluorescence

The X-ray fluorescence (XRF) for Magnesia-1 LS subsample is presented in (Fig. 1). The spectrum shows signals corresponding to Mg, Ca, and O, which provide direct evidence for magnesium presence on LS surface. Furthermore, the Figure identifies calcite as a major mineral constituent. The crystal structure of the native LS did not show any significant compositional changes after amendment.

Fourier transform infrared spectroscopy

The FTIR spectra of Magnesia and Magnesia-1 LS subsamples are presented in (Fig. 2). The FTIR of LS subsamples was characterized by the bands ($1420, 875, 710 \text{ cm}^{-1}$) indicating the presence of calcite (Harrison et al. 1998). The spectra also showed presence of organic compounds as indicated by the peaks $2500\text{--}3400 \text{ cm}^{-1}$.

The spectra for Magnesia and Magnesia-1 LS subsamples were similar except of the presence of small shift in frequencies 1418 cm^{-1} to 1422 cm^{-1} and the extra new sharp band which appeared in the spectrum 3699 cm^{-1} characterizing the O–H stretching vibration of monomeric form of $\text{Mg}(\text{OH})_2$ (Bakovic et al. 2006).

Fig. 1 Results of X-Ray fluorescence for Magnesia-1 LS subsample

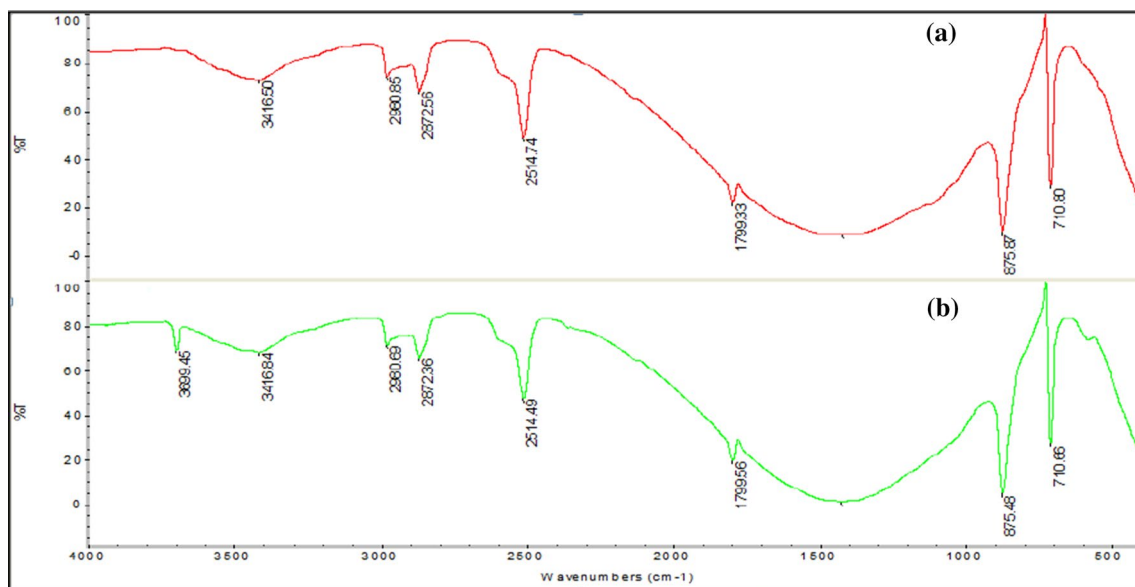
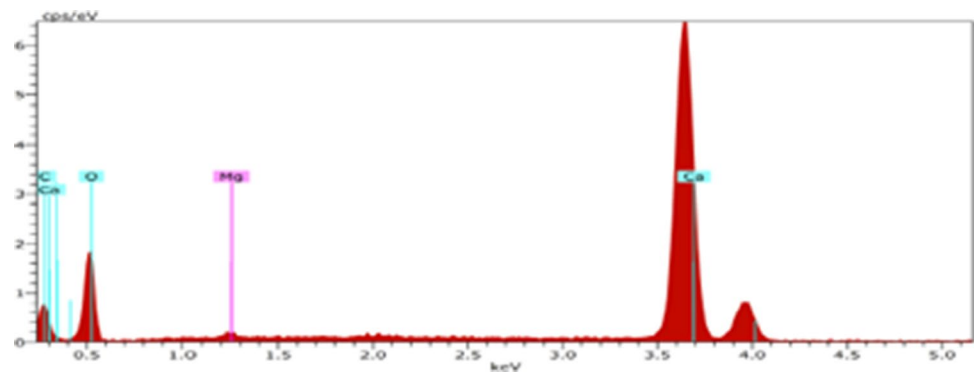


Fig. 2 Results of the FTIR analysis for **a** Magnesia, **b** Magnesia-1 LS subsamples

Figure 3 spectrum of the native and amended LS following F^- adsorption show that there were no major changes on native LS, while Magnesia-1 LS subsample shows that the particles surface functional groups significantly changed after the F^- adsorption. This indicates a chemical process to had taken place as evidenced by significant band shifting and certain peak intensity due to the F^- adsorption. Furthermore, additional peaks appeared in the high spectrum range $3200\text{--}3900\text{ cm}^{-1}$. The appearance of these peaks may have indicated a formation of various oxides, and thus, may reflect the complexity and heterogeneity of the adsorbing surface sites (Focke et al. 2009; Markovic et al. 2009). A new peak of 564.17 cm^{-1} was gradually formed. This new peak can be assigned to the $Mg\text{--}F$ stretching vibration, indicating the formation of MgF_2 during the adsorption process (Jin et al. 2016). The results of FTIR confirmed the presence of a ligand exchange of surface --OH by F^- . The 1420 cm^{-1} peak was shifted to 1387 cm^{-1} . These peaks belonged to the surface carbonate groups of native LS. The former shift

suggested that the ligand exchange had also taken place between carbonate groups and F^- (Zhang and Jia 2018; Yu et al. 2018).

Furthermore, pH measurements for F^- solutions at equilibrium was done after solid separation; and found that for native LS the pH remains constant at 8.22, which is the same pH value when water is in equilibrium with both CO_2 form the atmosphere and carbonate containing rock, while for amended LS (Magnesia-2) pH increased to 8.78 confirming OH^- release into the solution due to ligand exchange of surface-OH by F^- .

Surface area measurement

Results of surface area measurements for Magnesia and Magnesia-1 LS subsamples were similar ($2.10\text{ m}^2\text{ g}^{-1}$) the corresponding pore volume was $5.10 \times 10^{-3}\text{ cc g}^{-1}$. The respective results for Gama LS were $1.83\text{ m}^2\text{ g}^{-1}$ and $4.15 \times 10^{-3}\text{ cc g}^{-1}$. The relatively low surface areas were

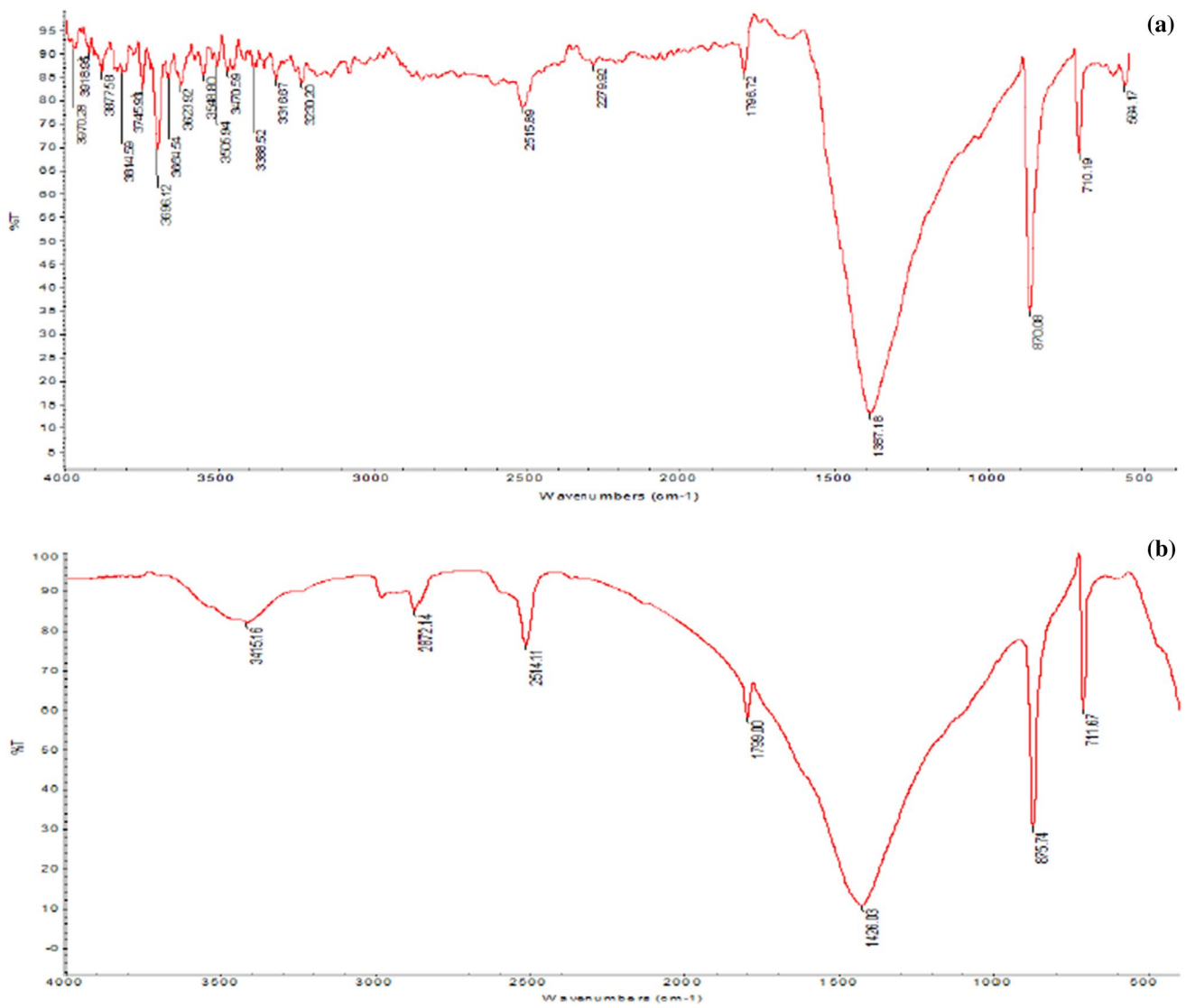


Fig. 3 FTIR spectrum for a Magnesia-1 b Magnesia LS following the F⁻ adsorption

Fig. 4 Scanning electron micrographs a Magnesia b Magnesia-1 LS subsamples

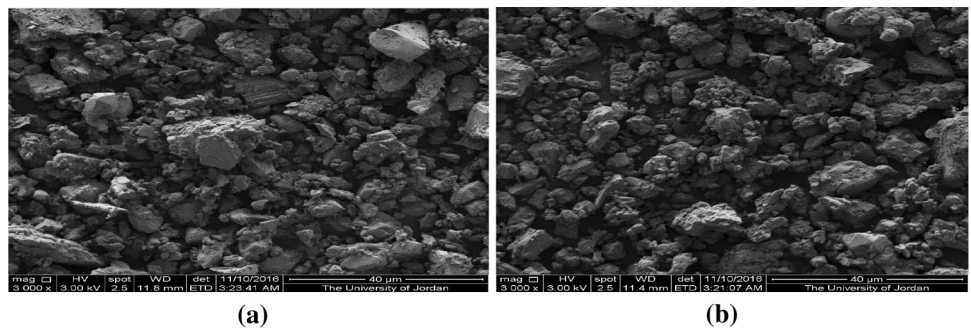


Table 2 Chemical analysis for Wadi Al-Yutum groundwater used in the study

Analysis	Value
Density(g ml ⁻¹)	1.0
pH	7.7
Conductivity (μS cm ⁻¹)	917.0
Turbidity (NTU)	0.3
mg L ⁻¹	
F ⁻	1.8
K ⁺	2.3
NO ₃ ⁻	22.0
Ca ⁺²	74.0
SO ₄ ⁻²	120.0
Na ⁺	130.0
TDS	642.0
Cl ⁻	230.0
Mg ⁺²	26.0
PO ₄ ⁻³	0.1
Total hardness as CaCO ₃	292.0

close to some values reported in literature (Bang et al. 2012; Liu and Yang 2015).

Scanning electron microscopy

Pictures of SEM of Magnesia and Magnesia-1 LS subsamples are shown in (Fig. 4a, b). Both figures show irregularly shaped particles with surface agglomerates of smaller particle sizes adhered to larger particles. There was no major difference in surface morphology of all samples. This was

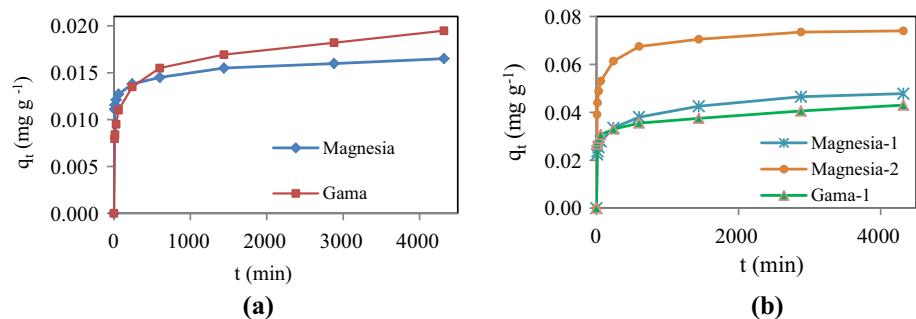
probably due to the relatively low suspension concentration and the rapid solid precipitation of Mg(OH)₂. These results were different from these of Jain and Jayaram (2009) which showed new aluminum hydroxide fibers that agglomerated the LS particles.

Characterization of Wadi Al-Yutum groundwater

Water samples from Wadi Al-Yutum wells were collected after flushing the pumps discharging line. Selected chemical and physical parameters were analyzed as shown in (Table 2). Results of the analysis showed slightly alkaline pH, predominance of SO₄⁻², Cl⁻ and Na⁺ ions, low PO₄⁻³ concentration and slightly high TDS, but lower than the WHO recommended maximum permissible level of 1,000 mg L⁻¹ (WHO 2008). A relatively high F⁻ concentration exceeding the allowable limit of 1.5 mg L⁻¹ was also reported.

Fluoride adsorption kinetics

Kinetics of F⁻ adsorption onto the native and amended LS subsamples are shown in (Fig. 5). Most of soluble F⁻ was removed from the aqueous phase within the first 60 min, but adsorption equilibrium was obtained after 72 h. The observed decreasing adsorption rate may have been due to the decreasing available sites for F⁻ adsorption with time. The Figure also shows that native and amended LS subsamples had different adsorption kinetics at the same experimental conditions. The maximum F⁻ adsorption corresponded to Magnesia-2 subsample. In

Fig. 5 Experimental F⁻ adsorption kinetics onto **a** native **b** amended LS subsamples**Table 3** Improvement on LS adsorption capacity due to adding OH functional group to LS surface

	% improvement on adsorption capacity	Source
Al(OH) ₃ -Impregnated LS	1.95	Jain and Jayaram, 2009
Mg(OH) ₂ -amended LS-single OH strength	2.94	This work
Mg(OH) ₂ -amended LS -double OH strength	4.5	This work

such a case, adsorption was 72% of the maximum capacity as compared to 16% for the native Magnesia and 47% for Magnesia-1 subsample.

Comparison for improvement on LS adsorption capacity due to addition of OH functional group from two different sources is presented in (Table 3). Results show higher improvement for Mg(OH)₂-amended LS compared with Al(OH)₃-modified LS. Additionally, this Ca and Mg-based adsorbent are nontoxic which eliminate threats of elevated Al concentrations in treated water.

The rate at which adsorption takes place is an important factor in designing any adsorption system (Worch 2012). In this study, results of F⁻ adsorption were tested against first-order and second-order kinetics, intra-particle diffusion, and Elovich models.

Determination of the best-fit kinetic model is usually carried out through analysis of the correlation coefficient (R^2) or the variance about the mean:

$$R^2 = \frac{\sum (q_m - q_{e,avg})^2}{\sum (q_m - q_{e,avg})^2 + \sum (q_m - q_e)^2} \quad (2)$$

where q_m is a constant obtained from the kinetic model, q_e is the equilibrium capacity obtained from experimental data, and $q_{e,avg}$ is the average of q_e . The coefficient of determination R^2 is based on the linear forms of the kinetic equations, but does not represent the errors in the kinetic curves. Although efficient, this indicator is limited to solving kinetic models of a linear form. Therefore, in this work three different error functions were employed to examine the best-fit model, i.e., the sum of square errors (SSEs), standard deviation of relative errors (SDs), and residual root mean square error (RMSE).

$$SSE = \sum \frac{(q_{e,expt} - q_{e,cal})^2}{q_{e,expt}} \quad (3)$$

$$RMSE = \sqrt{\frac{1}{n-2} \sum_{i=1}^n (q_{e,exp} - q_{e,cal})^2} \quad (4)$$

$$S.D.(%) = 100 \times \left\{ \frac{\sum (1 - (q_{t,cal}/q_{t,exp}))^2}{N} \right\}^{1/2} \quad (5)$$

where $q_{e,expt}$ and $q_{e,cal}$ are the experimental and the corresponding model-calculated values, respectively. If theoretical data were close to the respective experimental data then SSE, RMSE, and SD would have been small numbers.

First-order model

Fluoride adsorption (q_e , mg g⁻¹) can be calculated as:

$$q_e = \frac{(C_o - C_e)V_L}{m_A} \quad (6)$$

where q_e is the amount of ions adsorbed in (mg g⁻¹), C_o and C_e are the initial and equilibrium F⁻ concentrations (mg L⁻¹); m is the mass (g) of the adsorbent, and V is the volume of the solution (L). This can linearly be written as:

$$\log(q_e - q_t) = \log q_e - \frac{K_1}{2.303} t \quad (7)$$

where K_1 is the adsorption rate constant, q_e , and q_t are the amounts of adsorption at equilibrium and at time "t", respectively.

Adsorption results are shown in (Table 4). The coefficients of correlation were low and the error functions; SSE, RMSE, and especially SD were high and, thus, indicating that F⁻ adsorption did not conform to the first order model. This poor fitting of first order model to F⁻ adsorption data using native and amended LS indicates that the reaction is not inclined toward physisorption. First-order reaction is a reaction that proceeds at a rate that depends linearly on only one reactant concentration. Similar results of poor fitting of first order kinetic model to F⁻ adsorption onto calcite, quartz and fluorspar has been reported in literature (Fan et al. 2003).

Second-order model

The second-order kinetic is based on the assumption that adsorption is the rate limiting step:

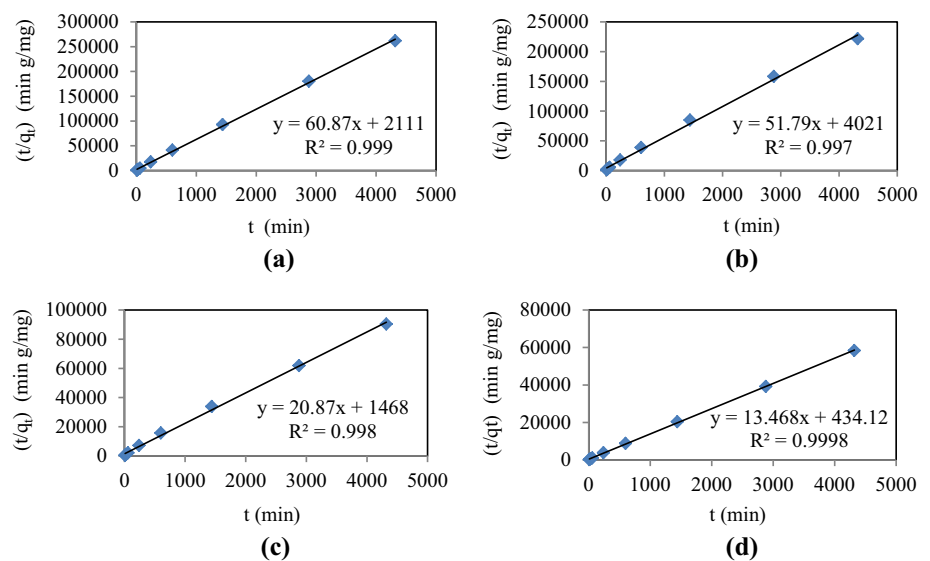
$$\frac{t}{q_t} = \frac{1}{K_2 q_e^2} + \frac{t}{q_e} \quad (8)$$

The rate parameter K_2 (g mg⁻¹ min⁻¹) and q_e can be directly obtained from the intercept and slope of the plot of t/q_t vs t (Fig. 6).

Second-order model was fit to the experimental data with high correlation coefficient ($R^2 > 0.99$) for all LS subsamples. This indicates that a chemical reaction was significant in that rate-controlling step. Similar results of F⁻ adsorption onto various adsorbents were reported by Nie et al. (2012). Here, adsorbed F⁻ formed a covalent chemical bond with calcium and magnesium replacing the functional groups on the adsorbent surface, where magnesium forms octahedral structure, while calcium forms tetrahedral structure (Graef and McHenry 2007). Therefore, adsorption is highly selective (ligand exchange) and

Table 4 Statistical parameters of kinetic models and their respective standard Error

Kinetic model	Parameter	Native LS		Amended LS		
		Magnesia	Gama	Magnesia-1	Magnesia-2	Gama-1
First order	q_e (mg g ⁻¹)	0.0051	0.0101	0.0246	0.0287	0.0161
	K_1 (mg g ⁻¹ min ⁻¹)	0.0009	0.0007	0.0012	0.0014	0.0007
	R^2	0.755	0.846	0.930	0.911	0.749
	RMSE	0.012	0.010	0.024	0.047	0.028
	SSE	0.094	0.072	0.168	0.347	0.221
	%SD	89.0	83.0	79.0	84.0	87.0
Second order	q_e (mg g ⁻¹)	0.016	0.019	0.048	0.074	0.042
	K_2 (g min ⁻¹ mg ⁻¹)	1.755	0.667	0.297	0.417	0.478
	R^2	0.999	0.997	0.998	0.999	0.997
	RMSE	0.004	0.003	0.009	0.011	0.010
	SSE	0.011	0.010	0.029	0.026	0.035
	%SD	33.0	36.0	37.0	26.0	37.0
Elovich	a (mg g ⁻¹ min ⁻¹)	22.15	0.01	0.06	1.35	72.63
	β (g mg ⁻¹)	0.0009	0.0019	0.0040	0.0050	0.0020
	R^2	0.998	0.998	0.991	0.983	0.974
	RMSE	0.0002	0.0002	0.0022	0.0050	0.0025
	SSE	2.E-05	3.E-05	1.E-03	3.E-03	1.E-03
	%SD	1.0	2.0	6.0	8.0	6.0
Intra-particle diffusion	c (mg g ⁻¹)	0.0095	0.0073	0.0195	0.0380	0.0224
	K_{id} (mg/g min ^{1/2})	0.0001	0.0002	0.0005	0.0010	0.0004
	R^2	0.432	0.740	0.712	0.550	0.506
	RMSE	0.0020	0.0019	0.0041	0.0126	0.0040
	SSE	0.0026	0.0023	0.0045	0.0200	0.0044
	%SD	15.0	14.0	12.0	18.0	12.0

Fig. 6 Second-order linearization for F⁻ adsorption onto **a** Magnesia **b** Gama **c** Magnesia-1 **d** Gama-1 LS subsamples

occurs only when chemically active surface sites are both numerous and available to the adsorbate chemical species.

Since no single Mg(OH)₂ solid phase was detected during the LS amendment with Mg(OH)₂, the most likely increase in F⁻ adsorption onto OH-amended LS subsamples was due

to adsorption onto the surface of Mg(OH)₂-coated LS particles. Surfaces of the Mg(OH)₂-amended LS subsamples were expected to become enriched with -OH functional groups as indicated by the FTIR and XRF results, and thus, ligand exchange is expected to have been the primary

adsorption mechanism (Art et al. 2020). Dissociation of $\text{Mg}(\text{OH})_2$ produces OH^- which is similar in charge and ionic radius to F^- :

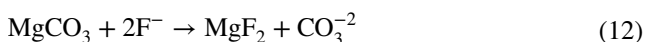


Possibility of MF (M is Ca or Mg ions) formations through ligand exchange was also reported by Rai et al. (2000):



This possibility was also supported by the FTIR results for the amended LS which showed significant changes following adsorption with multi peaks and band shifting in the high spectrum range ($3200\text{--}3900 \text{ cm}^{-1}$) characterizing the O–H stretching vibration of $\text{Mg}(\text{OH})_2$. In addition to the formation of the new peak at 564.17 cm^{-1} which can be assigned to the Mg–F stretching vibration. Some other research groups have considered this innovative approach and have univocally found out that vigorously homogenizing the experimental systems yields reproducible and relevant results for ion/ligand exchange mechanism (Devi et al. 2012; Margandan et al. 2014; Chigondo et al. 2018; Yu et al. 2018; Lee et al. 2017).

Possibility of $\text{LS}\text{-CO}_3$ ligand exchange with F^- was also supported by the FTIR results. Such exchange was reported by Yu et al. (2018) for surface- CO_3 of MgCO_3 :



Here, Mg^{2+} cations could co-precipitate with the hexagonal calcite crystal but in octahedral coordination with oxygen to form CaCO_3 solid phase solution (Morse et al. 2007; Smyth 1997). The well fit of the adsorption data for native LS ($R^2 > 0.99$) to second-order model can further support the ligand exchange hypothesis.

Intra-particle diffusion model

Intra-particle diffusion rate model assumes that the overall adsorption rate is controlled by the internal diffusion of the adsorbate:

$$q_t = K_{\text{id}} t^{1/2} + c \quad (13)$$

where c is a constant related to the thickness of the boundary layer (mg g^{-1}) and K_{id} is the intra-particle diffusion rate ($\text{mg g}^{-1} \text{ min}^{-1/2}$).

The calculated correlation coefficients for all adsorbents were low (0.4–0.7), i.e., experimental data did not fit to the model, despite the relatively low values of the error functions. In this regard, the model parameters essentially

depend on physical features of adsorbents, e.g., adsorbate diffusivity and adsorbent internal structure (Chakrapni et al. 2010). The surrounding operational conditions play minor role in the data conformity to the model. Rate constant values for native LS were very low as compared to the amended LS subsamples. Similarly, the "c" values were low, and thus, implied low-boundary layer effect. The highest value was reported for Magnesia-2 to be, followed by Magnesia-1 and Gama-1 LS subsamples as shown in (Table 4). Fitting results of intra-particle diffusion model confirm that F^- adsorption on native and amended LS was not limited by a diffusion step, but rather was affected by concentration of the reactants as earlier suggestion.

Elovich model

One of the most useful models describing chemical adsorption is the Elovich model (Wu et al. 2009):

$$q_t = \beta \ln(ab) + \beta \ln(t) \quad (14)$$

where a ($\text{mg g}^{-1} \text{ min}^{-1}$) is the initial adsorption rate and the parameter β (g mg^{-1}) is related to the extent of surface coverage by the adsorbate and required activation energy for the adsorption.

The plot of q_t against $\ln(t)$ produces the linear form. The results of adsorption kinetics conformed to the linear form of the above equation (Fig. 7) with low error functions and high correlation coefficient. The model implies that the most energetic sites will be occupied first. The model parameters; a and β were calculated and presented in (Table 4) which shows that the maximum " β " value $5.0 \times 10^{-3} \text{ g mg}^{-1}$ was that of Magnesia-2 LS subsample which also showed the maximum adsorption capacity compared to the value of $9.0 \times 10^{-4} \text{ g mg}^{-1}$ for Magnesia LS subsample.

Good fitting of experimental data to Elovich model is another evidence that the mechanism of F^- removal was a substitution of -OH by F^- on the amended LS surface. Both F^- and OH^- are isoelectronic and the ability of the former to coordinate with Ca^{2+} and Mg^{2+} ions is relatively higher than that with OH^- , supporting the possibility of ligand exchange at the surface of amended LS (Jin et al. 2016; Art et al. 2020).

Fluoride adsorption from Wadi Al-Yutum water

The background matrix effect of Wadi Al-Yutum well water on F^- adsorption can be envisaged as a result of potential competition of certain ions with F^- for the exchange sites. Fluoride adsorption kinetics from that water with $1.84 \text{ mg F}^- \text{ L}^{-1}$ were examined. Native and amended subsamples of both Magnesia and Gama were employed as adsorbents (Fig. 8). The results indicated

Fig. 7 Elovich linear plot of F⁻ adsorption onto **a** Gama **b** Magnesia **c** Magnesia-2 **d** Gama-1 LS subsample

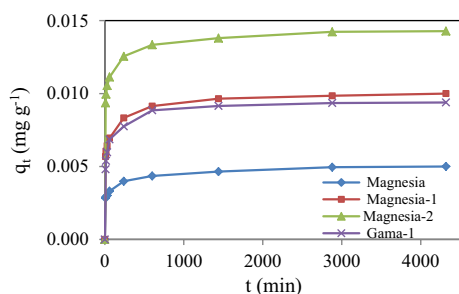
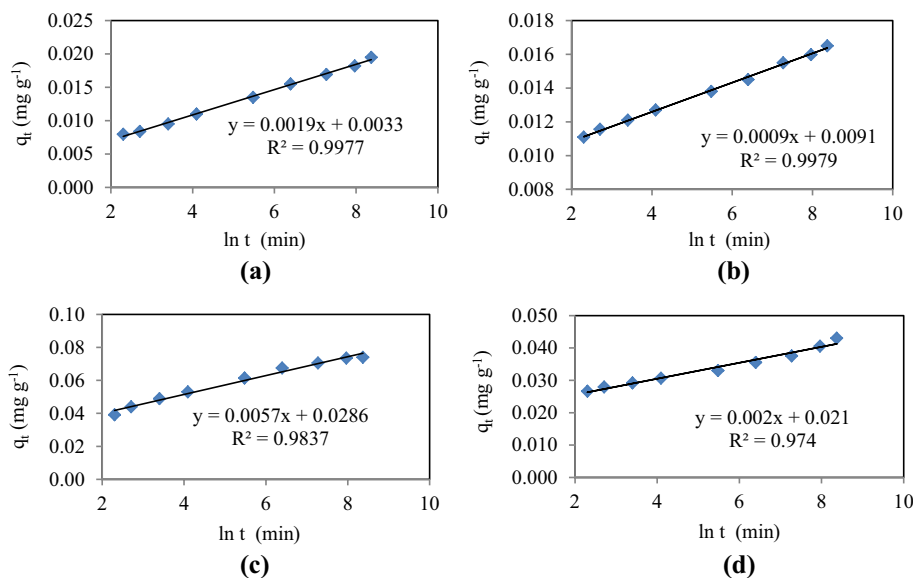


Fig. 8 Experimental F⁻ adsorption data using Wadi Al-Yutum groundwater

Table 5 Fluoride adsorption efficiency from Wadi Al-Yutum and F⁻ solution

Source	Native LS		Amended LS	
	Magnesia	Magnesia-1	Magnesia-2	Gama-1
Wadi Al-Yutum	27%	54%	77%	51%
F ⁻ solution	16%	47%	72%	42%

a significant increase in F⁻ adsorption onto Magnesia-2 within the first 10-min reaction. Native Magnesia LS subsample required 72 h to reduce F⁻ equilibrium concentration to 1.35 mg L⁻¹. Subsequently, maximum adsorption decreased in the order of Magnesia-2 (14 μg g⁻¹), Magnesia-1(10 μg g⁻¹) and Magnesia LS (5 μg g⁻¹).

Fluoride adsorption efficiency (E) from the well and synthetic solutions is presented in (Table 5). The "E" was calculated as:

$$E = \left[1 - \frac{C_e}{C_o} \right] * 100\% \tag{15}$$

where, C_o and C_e are initial and equilibrium F⁻ concentrations.

Fluoride adsorption efficiency values presented in (Table 5) shows that adsorption of F⁻ from the well water was not affected by the background ionic strength. However, F⁻ adsorption efficiency from the well water was even slightly higher than that from the synthetic solution. This slight increase may be due to faster adsorption from dilute solutions, as less F⁻ ions migrate to the adsorption sites in contrast to solutions with higher concentration. The high chloride concentration in the well water may have caused an increase in the repulsion forces which increasing F⁻ ions uptake (Chigondo et al. 2018). To the contrary, negligible effect of the coexisting ions of Cl⁻, SO₄⁻² and NO₃⁻ on F⁻ adsorption was reported in literature (Jin et al. 2016; Zhang and Jia 2018). Presence of HCO₃⁻, CO₃⁻² and PO₄⁻³ ions was reported to have adverse effect on F⁻ removal, especially at high concentrations (Nde-Tchoupe et al. 2019; Lee et al. 2017). The greater the charge density of a given anion (charge/radius) the more likely the anion is attracted to the adsorbent surface and hence the more it interferes with F⁻ ions adsorption. Concentration of PO₄⁻³ in the well water is low, and thus, the anticipated interference with F⁻ adsorption would be minimal. The same observation could be applied on SO₄⁻² which may further explain the minimal effect of the coexisting anions on F⁻ adsorption.

Evaluation of kinetic models

Similar to the previous results, adsorption kinetics conformed only to second-order and Elovich models. The

Fig. 9 Second-order linearization for F⁻ adsorption from Wadi Al-Yutum **a** Magnesia **b** Magnesia-1 **c** Magnesia-2 **d** Gama-1 LS subsamples

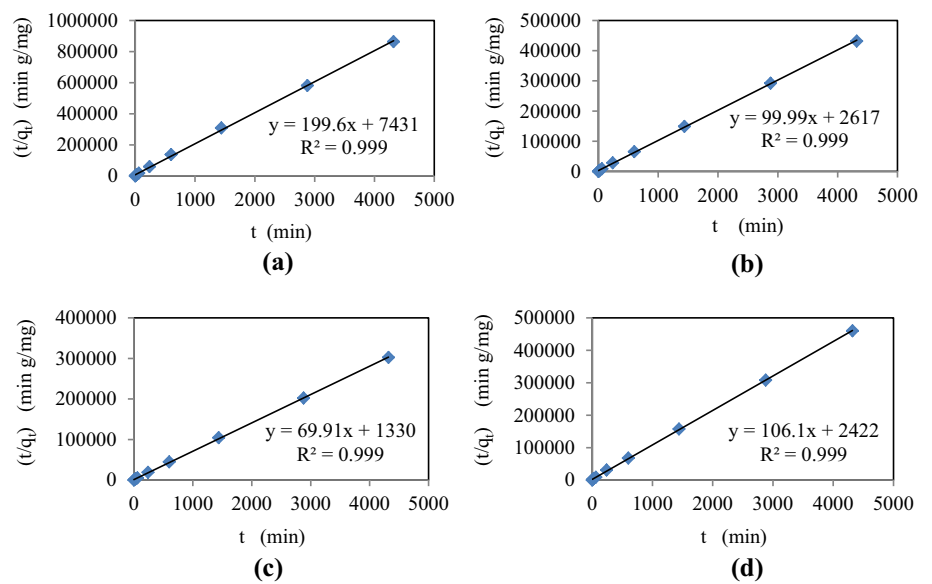
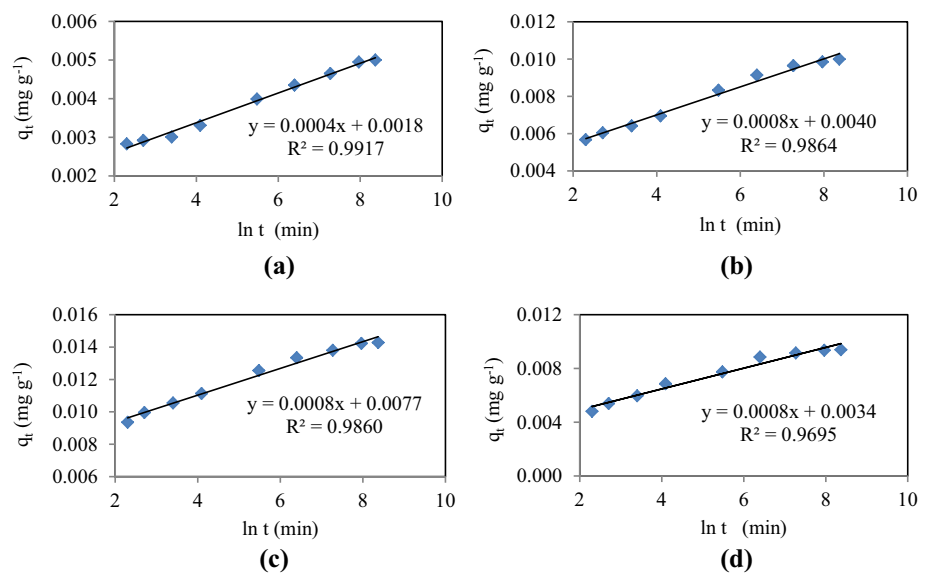


Fig. 10 Elovich Equation Linearization for F⁻ Adsorption from Wadi Al-Yutum **a** Magnesia **b** Magnesia-1 **c** Magnesia-2 **d** Gama-1 LS subsamples



results are presented in (Figs. 9 and 10). Improvement on F⁻ adsorption due to the presence of Mg(OH)₂ on LS surface was very clear since adsorption capacity for Magnesia-1 was nearly twice that for Magnesia LS, while Magnesia-2 showed nearly triple the adsorption capacity of Magnesia LS.

Conclusion

Limestone samples from two different locations in Central Jordan were used adsorbents for F⁻ removal from aqueous solutions. Adsorption was very rapid during the first 60 min then leveled-off gradually to reach equilibrium

after 72 h. The F⁻ adsorption data were best fitted to second-order and Elovich models, while did not fit to first order and intra-particle diffusion model. Adsorption of F⁻ onto Mg(OH)₂-amended LS subsamples was superior to native LS samples. The presence of the coating OH⁻ functional groups was hypothesized to form ligand exchange with F⁻ ions from the solution. Adsorption of F⁻ from Wadi Al-Yutum well water was not largely affected by the background ionic strength. However, LS amended subsamples were more effective in F⁻ removal from that water to ≤1 mg L⁻¹ within the first 10 min as compared to 1.35 mg L⁻¹ for native LS which required 72 h of continuous shaking.

Funding This research was partially supported by the Scientific Research Support Fund, Deanship of Academic Research, University of Jordan.

Compliance with ethical standards

Conflict of interest The authors declare that there are no conflicts of interest.

Open Access This article is licensed under a Creative Commons Attribution 4.0 International License, which permits use, sharing, adaptation, distribution and reproduction in any medium or format, as long as you give appropriate credit to the original author(s) and the source, provide a link to the Creative Commons licence, and indicate if changes were made. The images or other third party material in this article are included in the article's Creative Commons licence, unless indicated otherwise in a credit line to the material. If material is not included in the article's Creative Commons licence and your intended use is not permitted by statutory regulation or exceeds the permitted use, you will need to obtain permission directly from the copyright holder. To view a copy of this licence, visit <http://creativecommons.org/licenses/by/4.0/>.

References

- Abu-Sharar T (2005) Current and future challenges of water resources management in Jordan. *Jordan J Agric Sci* 1:1–15
- Ahn J (2012) Geochemical occurrences of arsenic and fluoride in bedrock groundwater: a case study in Geumsan County. *Korea Environ Geochem Health* 34:43–54
- Alagumuthu G, Veeraputhiran V, Venkataraman R (2010) Adsorption isotherms on fluoride removal: batch techniques. *Arch Appl Sci Res* 2:170–185
- Ali M (2013) Batch thermodynamics and kinetics study for removal of cationic dye from aqueous solution using Iraqi Limestone. *IOSR J Appl Chem* 4:11–20
- Aravind V, Elango K (2006) Adsorption of fluoride onto magnesium-equilibrium and thermodynamics study. *Indian J Chem Technol* 13:476–483
- Art J, Soumillion P, Dupont-Gillain C (2020) Use of a quartz crystal microbalance platform to study protein adsorption on aluminum hydroxide vaccine adjuvants: focus on phosphate-hydroxide ligand exchanges. *Int J Pharm* 573:811–834
- Bakovic S, Potgieter J, Waal D, Popovic L (2006) Replacing limestone and linseed oil in the synthesis of putty. *J Appl Sci* 6:1009–1016
- Bang J, Jang Y, Kim W, Song K, Jeon C, Chae S, Lee S, Park S, Lee M (2012) Specific surface area and particle size of calcium carbonate precipitated by carbon dioxide microbubbles. *Chem Eng J* 198:254–260
- Budyanto S, Kuo Y, Liu J (2015) Adsorption and precipitation of fluoride on calcite nanoparticles: a spectroscopic study. *Sep Purif Technol* 150:325–331
- Chakrapani C, Babu C, Vani K, Rao K (2010) Adsorption kinetics for the removal of fluoride from aqueous solution by activated carbon adsorbents derived from the peels of selected citrus fruits. *Eur J Chem* 7(1):419–427
- Chang M, Liu J (2007) Precipitation removal of fluoride from semi-conductor wastewater. *J Environ Eng* 133(4):419
- Chigondo M, Paumo H, Bhaumik M, Pillay K, Maity A (2018) Rapid high adsorption performance of hydrous cerium-magnesium oxides for removal of fluoride from water. *J Mol Liq* 265:496–509
- Davraz A, Sener E, Sener S (2008) Temporal variation of fluoride concentration in isparta public water system and health impact assessment (SW-Turkey). *Environ Geol* 56:159–170
- Devi R, Umlong I, Raul P, Das B, Banerjee S, Singh L (2012) Defluorination of water using nano-magnesium oxide. *J Exp Nanosci* 4:1–13
- Dutta R, Nath S (2010) Enhancement of limestone defluorination of water by acetic and citric acids in fixed bed reactor. *Clean: Soil, Air, Water* 38:614–622
- Ezzeddine A, Bedoui A, Hannachi A, Bensalah N (2015) Removal of fluoride from aluminium fluoride manufacturing wastewater by precipitation and adsorption processes. *Desal Water Treat* 54:2280–2292
- Fan X, Parker D, Smith M (2003) Adsorption kinetics of fluoride on low cost materials. *Water Res* 37:4929–4937
- Farhan Y, Anaba O (2016) Flash flood risk estimation of Wadi Yutum (Southern Jordan) Watershed using GIS based morphometric analysis and remote sensing techniques. *Open J Mod Hydrol* 6:79–100
- Focke W, Molefe D, Labuschagne F, Ramjee S (2009) The influence of stearic acid coating on the properties of magnesium hydroxide, hydromagnesite, and hydrotalcite powders. *J Mater Sci* 1:1–27
- Gbadebo A (2012) Groundwater fluoride and dental fluorosis in southwestern Nigeria. *Environ Geochem Health* 34:597–604
- Gmar S, Sayadi I, Helali N, Tlili M, Amor M (2015) Desalination and defluorination of tap water by electrodialysis. *Environ Process* 31:209–222
- Graef M, McHenry M (2007) Structure of material: an introduction to crystallography, diffraction, and symmetry. Cambridge University Press, New York
- Habuda-Stanic M, Ravancic M, Flanagan A (2014) A review on adsorption of fluoride from aqueous solution. *Material* 7:6317–6366
- Harrison D, Inglethorpe S, Mitchell C, Kemp S, Chaodumrong P, Charusribandhu M (1998) Procedures for the rapid assessment of limestone resources-technical report WC/98/1 overseas geology series. Br Geol Survey UK.
- Heimann S, Nde-Tchoupe A, Hu R, Licha T, Noubactep C (2018) Investigating the solubility of Fe⁰ packed-beds for water defluorination. *Chemosphere* 209:578–587
- Jain S, Jayaram R (2009) Removal of fluoride from contaminated drinking water using unamended and aluminium hydroxide impregnated blue lime stone waste. *Sep Sci Technol* 4:1–16
- Jayarathne A, Weerasooriya R, Chandrajith R (2015) A rapid method for the removal of fluoride in contaminated groundwater using natural crystalline apatite: a laboratory and field study. *Environ Earth Sci* 73:8369–8377
- Jin Z, Jia Y, Zhang K, Kong L, Sun B, Shen W, Meng F, Liu J (2016) Effective removal of fluoride by porous MgO nanoplates and its adsorption mechanism. *J Alloys Comp* 675:292–300
- Karro E, Uppin M (2013) The occurrence and hydrochemistry of fluoride and boron in carbonate aquifer system, central and Western Estonia. *Environ Monit Assess* 185:3735–3748
- Khichar M, Kumbhat S (2015) Defluorination: a review of water from aluminium and alumina based compound. *Int J Chem Stud* 2:4–11
- Lee S, Ha J, Sohn E, Park I, Lee S (2017) Synthesis of pillar and microsphere-like magnesium oxide particles and their fluoride adsorption performance in aqueous solutions. *Korean J Chem Eng* 34(10):2738–2747
- Liu Y, Yang Y (2015) Evolution of the surface area of limestone during calcination and sintering. *J Power Energy Eng* 3:56–62
- Ma W, Lv T, Song X, Cheng Z, Duan S, Xin G, Liu F, Pan D (2014) Characteristics of Selective Fluoride Adsorption By Biocarbon-Mg/Al layered double hydroxides composites from protein solutions: kinetics and equilibrium isotherms study. *J Hazard Mater* 268:166–176

- Margandan K, Agrawal R, Acharya R, Sharma S, Qanungo K (2014) Kinetics of fluoride removal from groundwater using MgO. *Chem Bull* 59(73):19–27
- Markovic M, Takagi S, Chow L, Frukhtbeyn S (2009) Calcium fluoride precipitation and deposition from 12 mmol/L fluoride solutions with different calcium addition rates. *J Res Natl Inst Stand Technol* 114:293–301
- Medellin-Castillo N, Leyva-Ramos R, Padilla-Ortega E, Perez R, Flores-Cano J, Berber-Mendoza M (2015) Adsorption capacity of bone char for removing fluoride from water solution. role of hydroxyapatite content, adsorption mechanism and competing anions. *J Ind Eng Chem* 20:4014–4021
- Mnif A, Ali M, Hamrouni M (2010) Effect of some physical and chemical parameters on fluoride removal by nanofiltration. *Ionics* 16:245–253
- Morse J, Arvidson R, Luttge A (2007) Calcium carbonate formation and dissolution. *Chem Rev* 107(2):342–381
- Nde-Tchoupe A, Nanseu-Njiki C, Hu R, Nassi A, Noubactep C, Licha T (2019) Characterizing the reactivity of metallic iron for water defluoridation in batch studies. *Chemosphere* 219:855–863
- Nie Y, Hu C, Kong C (2012) Enhanced fluoride adsorption using Al (III) amended calcium hydroxyapatite. *J Hazard Mater* 233:194–199
- Padhi S, Tokunaga T (2015) Surface complexation modeling of fluoride sorption onto calcite. *J Environ Chem Eng* 3:1892–1900
- Rai K, Agarwal M, Dass S, Shrivastava R (2000) Fluoride diffusive mobility in soil and some remedial measures to control its plant uptake. *Curr Sci* 79:1370–1373
- Smyth J (1997) The crystal structure of calcite III. *Geophys Res Lett* 24(13):1595–1598
- Tikki M (2014) Fluoride removal from water: a review. *Int J Sci Eng Res* 5:515–519
- Turner B, Binning P, Stipp S (2005) Fluoride removal by calcite: evidence for fluoride precipitation and surface adsorption. *Environ Sci Technol* 39:9561–9568
- Vences-Alvarez E, Velazquez-Jimenez L, Chazaro-Ruiz L, Diaz-Flores P, Rangel-Mendez J (2015) Fluoride removal in water by a hybrid adsorbent lanthanum-carbon. *J Coll Inter Sci* 455:194–202
- Vinati A, Mahanty B, Behera S (2015) Clay and clay minerals for fluoride removal from water: a state-of-the-art review. *Appl Clay Sci* 114:340–348
- Waghmare S, Arfin T (2015) Fluoride removal from water by various techniques: review. *Int J Innov Sci Eng Technol* 2(9):560–571
- Wang X, Yang H, Li Z, Yang S, Xie Y (2015) Pilot study for the treatment of sodium and fluoride contaminated groundwater by using high-pressure membrane systems. *Front Environ Sci Eng* 9:155–163
- Worch E (2012) Adsorption technology in water treatment fundamental, processes, and modeling. Walter de Gruyter GmbH & Co.KG, Berlin/Boston
- World Health Organization (2008) Guidelines for drinking water quality. World Health Organization, Geneva
- Wu F, Tseng R, Juang R (2009) Characteristics of elovich equation used for the analysis of adsorption kinetics in dye-chitosan systems. *Chem Eng J* 150:366–373
- Xu X, Li Q, Cui H, Pang J, An H, Zhai J (2012) Column-mode fluoride removal from aqueous solution by magnesia-loaded fly ash cenosphere. *Environ Technol* 33:1409–1415
- Yu Z, Xu C, Yuan K, Gan X, Zhou H, Wang X, Zhu L, Zhang G, Xu D (2018) Template-free synthesis of MgO mesoporous nanofibers with superior adsorption for fluoride and congo red. *Ceram Int* 44:9454–9462
- Zhang Y, Jia Y (2018) Fluoride adsorption on manganese carbonate: ion-exchange based on the surface carbonate-like groups and hydroxyl groups. *J Coll Inter Sci* 510:407–417

Publisher's note Springer Nature remains neutral with regard to jurisdictional claims in published maps and institutional affiliations.